Supercoiling transitions of closed DNA

Frank Jülicher
Institut für Festkörperforschung, Forschungszentrum Jülich, 52425 Jülich, Germany
(Received 3 November 1993)

Conformations of closed DNA molecules are considered within a simple elastic model. The interplay of elastic energies of bending and twisting can lead to supercoiling induced by variations of the linking difference. These shape transformations are studied in the limit of a large length to thickness ratio of the molecule. Stationary shapes and energy diagrams are obtained by solving shape equations for closed rings. Four different families of stationary shapes can be distinguished: (i) planar circles, (ii) nonplanar rings, (iii) self-interacting rings, and (iv) interwound configurations. They all occur as shapes of minimal energy in the phase diagram of supercoiling. The transitions between the different regions in this phase diagram can be either continuous or discontinuous. The sequence of shape transitions turns out to be sensitive to the precise values of the elastic parameters. The buckling instability of the circle changes within the range of physically accessible values from continuous to discontinuous behavior.

PACS number(s): 87.10.+e, 02.40.−k

I. INTRODUCTION

DNA molecules often occur as closed rings which can be observed in the electron microscope [1]. The ring closure fixes the topology of the two strands characterized by their linking number $\mathcal{L}$ [2,3]. Under the action of topoisomerases, which are enzymes that can change the linking number, topoisomers of different topology are generated. This phenomenon can be studied by gel electrophoresis where molecules with different linking number are separated [4]. The reason for this separation is different tertial structures of the topoisomers. Under an increase of the linking number, a flat configuration of the molecule will in general be transformed into a supercoiled state which is stabilized by an interplay of elastic energies and the topological constraint [2,5–10]. The mechanical properties of DNA can be approximated by those of an elastic rod [5–12]. In order to be compatible with a given linking number, the molecule either can form a supercoiled shape with increased bending energy, or it can twist, which leads to an increase of the torsional elastic energy. Therefore, the shape of a closed molecule depends on the relative strength of the elastic parameters for bending and torsional deformations. This competition of elastic parameters leads to a buckling instability of the circle which has been studied by different authors [6,8,9]. Furthermore, stable shapes of closed DNA have been calculated using shape equations [6,7,9] and finite element computer simulations [10].

In this paper, a simple elastic model for closed DNA is studied systematically. The basic simplifying assumptions are (i) that the molecule behaves like a homogeneous elastic rod with bending and torsional rigidities and (ii) that the ratio of the length S_0 to the thickness a of the rod is large. The latter assumption becomes important for self-interacting shapes where self-avoidance acts as an additional constraint. The complete phase diagram for this model is derived using energy diagrams which are obtained by solving the Euler-Lagrange equations of the energy functional. Within the phase diagram of the model, different types of stable shapes can be distinguished: (i) planar circles, (ii) nonplanar rings, (iii) self-interacting rings, and (iv) interwound configurations. The phase diagram exhibits a rich structure of shape transitions between different types of shapes which are either continuous or discontinuous. Their properties depend significantly on the values of the elastic constants of the rod. The buckling transition of circular shapes changes from continuous to discontinuous behavior within the range of physically accessible values of the elastic constants.

The paper is organized as follows. The basic mathematical concepts to describe the geometrical properties of DNA are introduced in Sec. II. The physical model is defined in Sec. III. In order to obtain stationary shapes, variational methods are used which are described in Sec. IV. The complete phase diagram is derived in Sec. V. In Sec. VI, the results of the theory are related to those geometrical and elastic properties of DNA which have been measured experimentally. The Appendixes give some technical details. In Appendix A, the shape equations are derived. Boundary conditions for self-interacting shapes are discussed in Appendix B.

II. GEOMETRY AND TOPOLOGY OF CLOSED DNA MOLECULES

DNA molecules are large polymers which consist of two strands forming a double helix. The geometry of this double helix can be modeled by a twisted ribbon as shown in Fig. 1 [2,8]: The axis of the ribbon is given by the molecular axis with coordinates $\mathbf{R}(S)$ parametrized by the arclength S. Along the axis $\mathbf{R}(S)$, we define two unit vectors $\mathbf{t}$ and $\mathbf{u}$. The tangent vector $\mathbf{t}$ obeys $\mathbf{t}(S) = \dot{\mathbf{R}}(S)$, where the overdot denotes a derivative with respect to

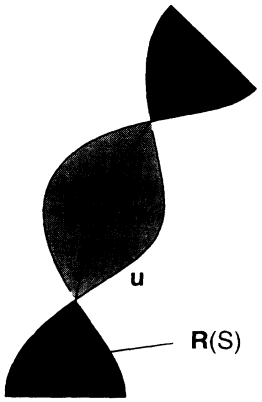

FIG. 1. Twisted ribbon as a model for the geometrical properties of DNA. The central line of the ribbon follows the molecular axis with coordinates $\mathbf{R}(S)$ parametrized by the arclength S. Two unit vectors are defined along the axis: the tangent vector $\mathbf{t}$ and the vector $\mathbf{u}$ perpendicular to $\mathbf{t}$ which points to the edge of the ribbon.

the arclength S. The vector $\mathbf{u}(S)$ is orthogonal to $\mathbf{t}(S)$ and points from the axis to the edge of the ribbon.

The topology of a closed DNA molecule can be characterized by its linking number $\mathcal{L}$, which is an integer counting the number of times the helix winds around the axis. White's formula [2,13]

$$\mathcal{L} = \mathcal{T}[\alpha(S)] + \mathcal{W}[\mathbf{R}(S)] \tag{1}$$

expresses the linking number $\mathcal{L}$ as a sum of two geometrical quantities, the twist $\mathcal{T}$, and the writhing number $\mathcal{W}$. Both $\mathcal{T}$ and $\mathcal{W}$ are in general not integers and depend on specific geometrical properties of the closed ribbon. The twist $\mathcal{T}$, with [2,8]

$$\mathcal{T} \equiv \frac{1}{2\pi}\int_0^{S_0} dS\, \alpha(S) \quad , \tag{2}$$

is a functional of the helicity

$$\alpha \equiv (\mathbf{t}\times\mathbf{u})\cdot\frac{d\mathbf{u}}{dS} \quad . \tag{3}$$

S_0 is the length of the molecule.

The writhing number $\mathcal{W}$ characterizes the shape of the curve $\mathbf{R}(S)$. It can be expressed by a double integral [2]

$$\mathcal{W} \equiv \frac{1}{4\pi}\int_0^{S_0}\int_0^{S_0} \times dS_1\, dS_2\, \frac{[\mathbf{t}(S_1)\times\mathbf{t}(S_2)][\mathbf{R}(S_1)-\mathbf{R}(S_2)]}{|\mathbf{R}(S_1)-\mathbf{R}(S_2)|^3} \tag{4}$$

and is defined only for curves which do not self-intersect. For a DNA molecule, a self-intersection of the molecular axis is avoided, since two segments of the molecule cannot interpenetrate.

III. ELASTIC ENERGY

While the geometrical properties of DNA are best represented by a twisted ribbon, its elastical properties are in a simple model those of a homogeneous elastic rod along the curve $\mathbf{R}(S)$ [5–12]. The total energy of an elastic rod is given by the sum [14] $F \equiv F_B + F_T$ of the bending energy

$$F_B \equiv \frac{B}{2}\int_0^{S_0} dS\, c(S)^2 \tag{5}$$

and the energy of torsional deformations

$$F_T \equiv \frac{C}{2}\int_0^{S_0} dS\, [\alpha(S)-\alpha_0]^2 \quad . \tag{6}$$

The bending rigidity and the torsional rigidity are denoted B and C, respectively. The curvature $c(S) = \sqrt{\dot{\mathbf{t}}^2}$ along the curve $\mathbf{R}(S)$ describes bending deformations of the rod. Torsional deformations lead to a nonvanishing physical torsion $\alpha(S) - \alpha_0$. Here α_0 is the helicity of the DNA molecule in the torsionally relaxed state [2,5,12,15]. For a molecule of length S_0, this helicity corresponds to $\mathcal{L}_0 \equiv \alpha_0 S_0/(2\pi)$ windings of the helix around the molecular axis.

IV. ENERGY MINIMIZING SHAPES

The physical state of a closed DNA molecule is defined by the shape of its axis $\mathbf{R}(S)$ together with the torsional deformation $\alpha(S) - \alpha_0$. Neglecting thermal fluctuations, the molecule attains a shape which has a minimal total energy F for given linking number $\mathcal{L}$. The constraint on $\mathcal{L}$ leads to an effective coupling of bending and torsional deformations as described by White's formula (1). The two relevant dimensionless parameters of this problem are (i) the linking difference

$$\Delta\mathcal{L} \equiv \mathcal{L} - \mathcal{L}_0 \tag{7}$$

and (ii) the ratio C/B of the two elastic parameters.

The phase diagram of this model can be obtained in two steps. First, the limit of large torsional rigidity C is studied. In this case, the torsional energy effectively acts as a constraint on the writhing number $\mathcal{W}$. Second, once this special case is solved, the energies and the shapes that correspond to arbitrary values of the torsional rigidity C can be obtained by applying a generalized Legendre transformation.

This procedure is carried out in Secs. IV A–IV C. In Sec. IV A, the bending energy F_B is minimized for given writhing number $\mathcal{W}$. Two different branches of stationary shapes which are obtained as solutions of the corresponding variational problem are discussed in Sec. IV B. In Sec. IV C, a generalized Legendre transformation is introduced. This transformation will be used in Sec. V to derive the complete phase diagram.

A. Minimal bending energy for fixed writhing number

For a torsionally stiff rod with large rigidity C, the helicity of a configuration which minimizes the total energy F is given by $\alpha(S) = \alpha_0$. This corresponds to a torsionally unstressed state which is governed by bending

energy $F = F_B$ only. The twist of this configuration is $\mathcal{T} = \mathcal{L}_0$. The constraint of fixed linking number $\mathcal{L}$ thus transforms into the constraint $\mathcal{W} = \Delta\mathcal{L}$ on the writhing number, as follows from White's formula (1).

Shapes that minimize the bending energy F_B for fixed writhing number $\mathcal{W}$ are obtained as stationary solutions of the functional

$$F' \equiv F_B + \gamma\mathcal{W} \quad . \tag{8}$$

Here γ is a Lagrange multiplier which has been introduced to incorporate the constraint on $\mathcal{W}$. In order to obtain Euler-Lagrange equations for this functional, it is convenient to use an expression for $\mathcal{W}$ which is local. The definition given in (4) is nonlocal and thus not useful for this purpose. Applying White's formula (1) to the curve $\mathbf{R}(S)$ with the special choice $\alpha = \tau$, where $\tau = \mathbf{t}\cdot(\dot{\mathbf{t}}\times\ddot{\mathbf{t}})/\dot{\mathbf{t}}^2$ is the differential geometrical torsion, the writhing number $\mathcal{W}$ can be written as [13]

$$\mathcal{W} = -\frac{1}{2\pi}\int_0^{S_0}\tau(S)\,dS + \mathcal{S} \quad . \tag{9}$$

This representation decomposes $\mathcal{W}$ into a sum of an integral over τ and a nonlocal part, the so-called self-linking number $\mathcal{S}$ [13,16]. The self-linking number is an integer quantity which, in general, does not change with small variations of the curve $\mathbf{R}(S)$. It will therefore be omitted as a constant contribution to F' [17].

With this representation of $\mathcal{W}$, the functional F' can be expressed as

$$F' = \int_0^{S_0} dS\left[\frac{B}{2}\dot{\mathbf{t}}^2 + \frac{\gamma}{2\pi}\frac{\mathbf{t}\cdot(\dot{\mathbf{t}}\times\ddot{\mathbf{t}})}{\dot{\mathbf{t}}^2} + \mathbf{N}(\dot{\mathbf{R}}-\mathbf{t})\right] \quad . \tag{10}$$

The additional vector $\mathbf{N}$ of Lagrange multipliers has been introduced in order to incorporate the contraint $\dot{\mathbf{R}} = \mathbf{t}$ on the coordinates $\mathbf{R}$. This is important since boundary conditions on both $\mathbf{R}$ and $\mathbf{t}$ have to be imposed. The condition $\delta F' = 0$ determines the shape equations as described in Appendix A.

B. Branches of solutions

Stationary shapes are obtained as solutions of the shape equations (A5) together with appropriate boundary conditions. They form one-dimensional branches which can be parametrized by the writhing number $\mathcal{W}$. Using the boundary conditions

$$\mathbf{R}(0) = \mathbf{R}(S_0), \quad \mathbf{t}(0) = \mathbf{t}(S_0), \quad \dot{\mathbf{t}}(0) = \dot{\mathbf{t}}(S_0) \quad , \tag{11}$$

which guarantee the smooth closure of the ring, one obtains a branch of nonplanar rings with $0 \le \mathcal{W} < 1$; see Fig. 2. For $\mathcal{W} = 0$, this branch starts with the circle $L_{\rm circ}$ with $E_B = 2\pi^2 B/S_0$. Shapes with finite $\mathcal{W}$ are nonplanar and begin to supercoil. As an example, the projections of the shape with $\mathcal{W} = 0.5$ on the X-Y plane, the X-Z plane, and the Y-Z plane are shown in Fig. 3(a). For $\mathcal{W} = 1$ the branch ends up with a singular limit shape $L_{\rm si}$. The shape $L_{\rm si}$ again is planar and begins to self-intersect; see Fig. 2(b). For finite rod thickness a, this limit shape is not reached because the chain would interpenetrate itself. The shape $L_{\rm si}$ therefore represents the onset of self-interaction in the limit of small a.

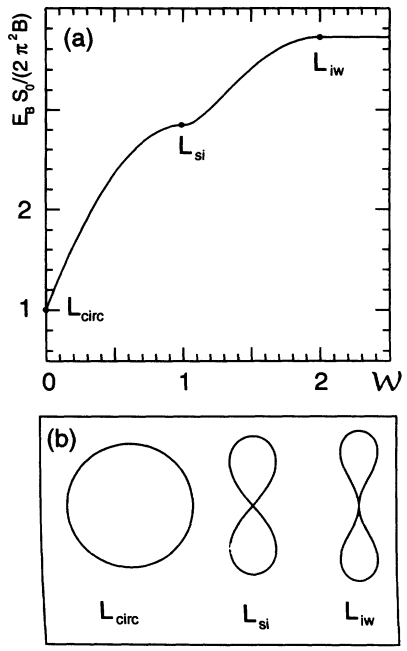

FIG. 2. (a) Bending energy E_B of stationary shapes as a function of the writhing number $\mathcal{W}$. For $\mathcal{W} = 0$, the branch starts with the circle $L_{\rm circ}$. The energy increases monotonically with $\mathcal{W}$. For integer values $\mathcal{W} = 1$ and $\mathcal{W} = 2$ of the writhing number, the planar limit shapes $L_{\rm si}$ and $L_{\rm iw}$ are reached, respectively. (b) Limit shapes $L_{\rm circ}$, $L_{\rm si}$, and $L_{\rm iw}$ corresponding to integer values of the writhing number $\mathcal{W} = 0$, 1, and 2 are shown. These shapes are planar and can therefore be displayed as two-dimensional contours.

Shapes with $\mathcal{W} > 1$ are not obtained with the branch discussed above since those shapes self-interact. In the most simple case of a pure hard core interaction, self-interacting configurations are stationary shapes with the

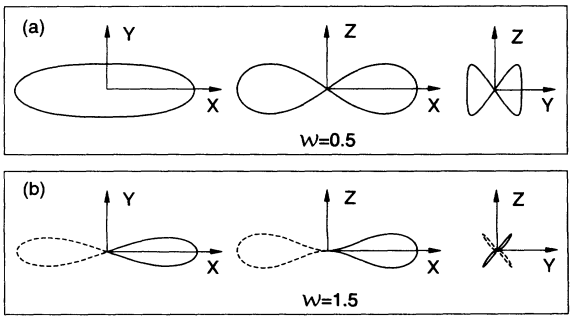

FIG. 3. (a) Projections of the nonplanar ring with $\mathcal{W} = 0.5$ on the X-Y plane, the X-Z plane, and the Y-Z plane, respectively. (b) The same projections for the self-interacting ring with $\mathcal{W} = 1.5$.

additional constraint of self-avoidance of the rod. For small rod thickness a, the region of self-interaction and self-contact of the rod reduces to a point. In this point, self-avoidance restricts the allowed variations of the rod. As described in Appendix B, this restriction corresponds to modified boundary conditions for the shape equations, which have to be imposed at the point of self-contact.

Together with these boundary conditions (B3)–(B7) for self-interacting shapes, the shape equations lead to a second branch of stationary shapes with $1 < \mathcal{W} < 2$ [18]. This branch starts for $\mathcal{W} = 1$ with the limit shape $L_{\rm si}$. As an example for a shape along this branch, three projections of the shape with $\mathcal{W} = 1.5$ are shown in Fig. 3(b). The branch ends up at $\mathcal{W} = 2$ with a new limit shape $L_{\rm iw}$ shown in Fig. 2(b). This shape $L_{\rm iw}$ is again planar and represents the onset of interwound configurations which are shapes, where the rod winds around itself at least once. It consists of two identical loops which are connected in the point of self-contact as shown in Fig. 2(b). Interwound configurations with $\mathcal{W} > 2$ are described by the same two loops but rotated with respect to each other by the angle $\Psi = (\mathcal{W} - 2)/\pi$ around the vertical symmetry axis; see Fig. 2(b). They have the same energy E_B as $L_{\rm iw}$ and exist with arbitrary values of $\mathcal{W} \geq 2$. However, only for $\mathcal{W} \simeq 2$ they would give a good description of interwound shapes for finite rod thickness a. The energy E_B of the two branches is shown as a function of $\mathcal{W}$ in Fig. 2(a) [19].

C. Generalized Legendre transformation

Shapes of minimal bending energy $E_B(\mathcal{W})$ for given writhing number $\mathcal{W}$ are now used to solve the complete problem, namely, to minimize the total energy $F = F_B + F_T$ for given linking number $\mathcal{L}$. First, the energy $E_T(\mathcal{T})$ is defined to be the minimum of the torsional energy F_T for all configurations $\alpha(S)$ with given twist $\mathcal{T}$. Using Eqs. (2) and (6), a simple calculation leads to [8]

$$E_T(\mathcal{T}) = \frac{2\pi^2 C}{S_0}(\mathcal{T} - \mathcal{L}_0)^2 \quad . \tag{12}$$

The total energy E of a stationary configuration with given linking number $\mathcal{L}$ can now be expressed as

$$\begin{aligned} E &= E_B(\mathcal{W}') + E_T(\mathcal{L} - \mathcal{W}') \\ &= E_B(\mathcal{W}') + \frac{2\pi^2 C}{S_0}(\Delta\mathcal{L} - \mathcal{W}')^2 \quad . \end{aligned} \tag{13}$$

Here the minimization of bending and torsional energy have been carried out independently and White's formula (1) has been used to incorporate the topological constraint. The writhing number $\mathcal{W}'$ satisfies the equation

$$\left.\frac{\partial E_B}{\partial \mathcal{W}}\right|_{\mathcal{W}=\mathcal{W}'} = \frac{4\pi^2 C}{S_0}(\Delta\mathcal{L} - \mathcal{W}') \quad , \tag{14}$$

which describes stationarity of the energy E in (13) with respect to variations of the writhing number $\mathcal{W}'$. Once the energy $E_B(\mathcal{W})$ has been determined, the total energy $E(\Delta\mathcal{L})$ of stationary configurations for any finite C can be obtained by the generalized Legendre transformation as given by Eqs. (13) and (14) [20]. For infinite C, Eq. (14) simplifies to $\mathcal{W}' = \Delta\mathcal{L}$, which was already observed in Sec. IV A.

V. PHASE DIAGRAM OF SUPERCOILING

The phase diagram of supercoiling is derived from diagrams of the energy $E(\Delta\mathcal{L})$ for different choices of C/B. These energy diagrams are obtained by applying the generalized Legendre transformation (14) to the function $E_B(\mathcal{W})$. Figure 4(a) shows the total energy E as a func-

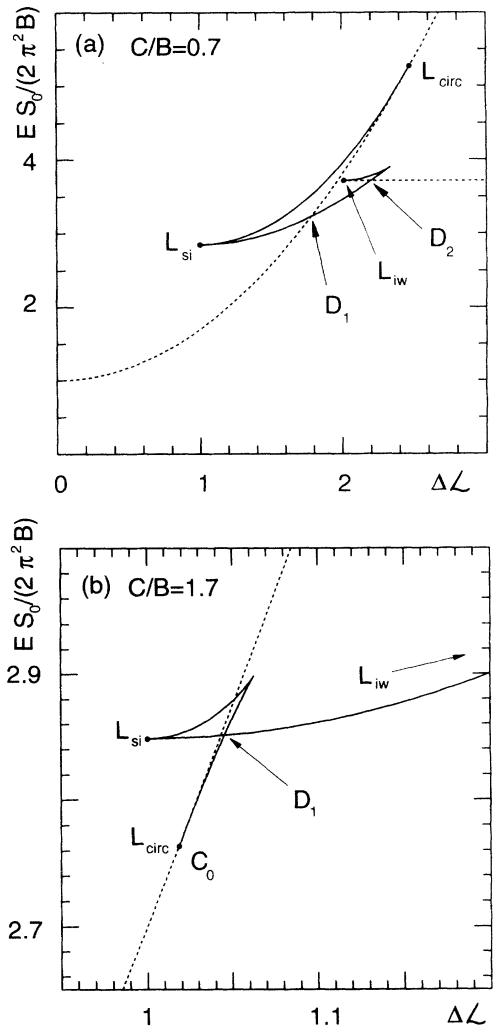

FIG. 4. (a) Total energy E as a function of the linking difference $\Delta\mathcal{L}$ for $C/B = 0.7$. The dotted parabola represents the energy of the circle. At the point $L_{\rm circ}$, the branch of nonplanar rings bifurcates from the parabola of circles. Two discontinuous transitions occur at the points D_1 and D_2. Between these two points, the branch of self-interacting shapes has the lowest energy. The planar limit shapes at both ends of this branch are denoted $L_{\rm si}$ and $L_{\rm iw}$. (b) The total energy for $C/B = 1.7$. In this case, the bifurcation of the nonplanar rings at $L_{\rm circ}$ leads to a continuous transition C_0. This transition is, for increasing $\Delta\mathcal{L}$, followed by a discontinuous transition D_1 to self-interacting shapes.

tion of $\Delta\mathcal{L}$ for $C/B = 0.7$. The circle with $\mathcal{W} = 0$ is always stationary for any value of $\Delta\mathcal{L}$ with energy $E = E_B(0) + 2\pi^2 C\Delta\mathcal{L}^2/S_0$. This line is shown as a dashed parabola. At the point $L_{\rm circ}$, the branch of nonplanar rings bifurcates from the parabola of planar circles. This branch is unstable for $C/B = 0.7$ and ends in the limit shape $L_{\rm si}$. At this point the branch of self-interacting rings starts, which is locally stable within a large range of $\Delta\mathcal{L}$. It ends up at the limit shape $L_{\rm iw}$. The dotted line with constant energy, which starts in the point $L_{\rm iw}$, describes interwound shapes with $\mathcal{W} > 2$. The discontinuous transitions D_1 and D_2 correspond to the crossing of the branch of self-interacting rings with the dotted parabola of circles and with the line of interwound shapes, respectively. The corresponding sequence of lowest energy shapes with increasing $\Delta\mathcal{L}$ is (i) circles, (ii) self-interacting rings, and (iii) interwound configurations.

The energy E versus $\Delta\mathcal{L}$ is shown for $C/B = 1.7$ in Fig. 4(b). Here the bifurcation of the nonplanar rings at $L_{\rm circ}$ leads to a stable branch. Therefore a continuous shape transition occurs at C_0. It is followed by a discontinuous transition D_1 of nonplanar rings to self-interacting rings. The branch of self-interacting rings ends up at $\Delta\mathcal{L} = 2$ with the limit shape $L_{\rm iw}$. At this point, a continuous transition C_2 between self-interacting rings and interwound shapes occurs.

The complete phase diagram is shown in Fig. 5. The two relevant variables are the absolute linking difference $|\Delta\mathcal{L}|$ [21] and the ratio C/B of the two elastic parameters. Four different regions can be distinguished within the phase diagram: (i) a region of circles with $\mathcal{W} = 0$, (ii) a region of nonplanar rings with $0 < \mathcal{W} < 1$, (iii) a region of self-interacting rings with $1 < \mathcal{W} < 2$, and (iv) a region of interwound configurations with $\mathcal{W} > 2$. While for large values of C/B all transitions are continuous, they all become discontinuous for sufficiently small values of C/B. This behavior also holds true for the buckling transition of the circle. Previous studies predicted this instability to occur along a line C_0 with $C/B = \sqrt{3}/|\Delta\mathcal{L}|$ [6,8]. The phase diagram shows that this statement is correct for $C/B \gtrsim 1.62$, where a continuous buckling instability occurs along the line C_0. For $C/B \lesssim 1.62$, however, this transition turns out to be discontinuous along the line D_1. The order of the transition changes at the critical end point CE where infinitesimally deformed circles become unstable. The three different discontinuous transition lines D_1, D_2, and D_3 meet at the point DE. The discontinuous transition lines D_1 and D_2 end up in the tricritical points TP_1 and TP_2, where the transitions become continuous along the lines C_1 and C_2 with $|\Delta\mathcal{L}| = 1$ and $|\Delta\mathcal{L}| = 2$, respectively.

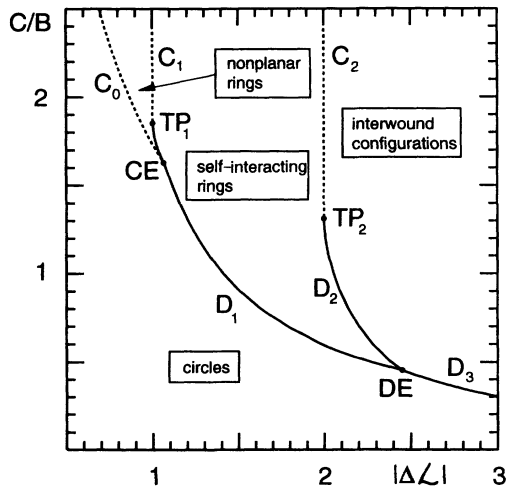

FIG. 5. Phase diagram for supercoiling. The two relevant parameters are the absolute linking difference $|\Delta\mathcal{L}|$ and the ratio of the two elastic parameters C/B. Four different reagions can be distinguished: (i) a region of circles, (ii) a region of nonplanar rings, (iii) a region of self-interacting rings, and (iv) a region of interwound configurations. Transitions between these regions are continuous along the dotted lines C_0, C_1, and C_2 and discontinuous along the lines D_1, D_2, and D_3. For an explanation of the other symbols, see the text.

VI. DISCUSSION

The topological constraint present in closed DNA molecules effectively couples bending and twisting deformations as described by White's formula. This interplay of elastic energies stabilizes supercoiled shapes for sufficiently large absolute linking difference $|\Delta\mathcal{L}|$. The corresponding shapes and shape transitions of closed DNA have been studied systematically for a simplified elastic model. In this model, the DNA is described as a homogeneous rod with bending and torsional elasticity. Self-interaction is included by a steric self-avoidance of the rod which is taken to be infinitely thin. Stable shapes are obtained as shapes of minimal total energy for fixed linking difference $\Delta\mathcal{L}$ by solving Euler-Lagrange equations for the shape of the molecular axes. The energies of stationary shapes for different values of the elastic parameters are related by a generalized Legendre transformation. The stability properties of stationary shapes can be checked by close inspection of the energy diagrams. Using these methods, the complete phase diagram as shown in Fig. 5 has been derived.

This simplified model applies for DNA molecules which are homogeneous along their axes. Higher order terms of the elastic energies which can become relevant for strong deformations have been neglected. A further simplification is the restriction to a steric self-avoidance of self-interacting configurations, thus neglecting adhesion energies and interaction potentials between different segments. For molecules with a length large compared to the persistence length $L_p \simeq 500$ Å [12,22], thermal fluctuations and entropy become important, which has been neglected in this study.

The model restricts to molecules which are long compared to their diameter $a \simeq 24$ Å [1]. However, the main results presented in this paper are unchanged for finite rod thickness a, since in this case the topology of the phase diagram will not change within the parameter range that has been investigated. The reason is that for a

rod with small diameter a, the energies of self-interacting shapes are changed by corrections of the order of $\sim a/S_0$, which only leads to small shifts of the phase boundaries. An important effect, however, arises for larger values of $|\Delta\mathcal{L}|$: For a rod with finite diameter, the bending energy of interwound configurations increases as a function of the writhing number $\mathcal{W}$. This can lead to additional transitions between interwound shapes which differ in their degree of supercoiling. These transitions are expected to occur close to integer values $|\Delta\mathcal{L}| \simeq 3, 4, \ldots$.

In order to apply this theory to observations of the shape changes of DNA molecules, the knowledge of the values of the elastic parameters is crucial. The bending rigidity B and the torsional rigidity C have both been determined in different studies [12,22]. Typical values for the torsional rigidity are $C \simeq (2-4)\times 10^{-19}$ erg cm. The bending rigidity is related to the persistence length by $B = L_p kT$, which leads to $B \simeq 2\times 10^{-19}$ erg cm. Here k is Boltzmann's constant and T denotes temperature. Physically accessible values for the ratio of the elastic parameters are therefore $C/B \simeq 1-2$. Inspection of the phase diagram shows that within the corresponding range, the sequence of shape transitions is very sensitive to the precise values of the elastic parameters.

The shape changes studied in this paper should be observable experimentally by varying the linking difference. This can be performed by different methods. Under the action of topoisomerases, one strand is cut and again reconnected, which leads to a change of the linking difference $\Delta\mathcal{L}$ by an integer amount [1,4,15]. In order to vary the linking difference continuously, ethidium bromide can be used. This is a dye molecule that tends to be inserted into the double helix, lowering the helicity α_0 of the DNA. An increase of the ethidium bromide concentration thus decreases the linking difference $\Delta\mathcal{L}$ continuously [15].

In conclusion, the topological coupling of bending and twisting, which leads to supercoiling of closed DNA molecules, has been studied in detail. The restriction to a simplified model allows the derivation of the complete phase diagram by using well established variational methods. The study reveals a complex structure of shape transitions and thus gives a deeper insight into the geometry and energetics of supercoiled DNA.

ACKNOWLEDGMENTS

I thank U. Seifert, C. Hiergeist, and R. Lipowsky for useful discussions and U. Seifert for a critical reading of the manuscript.

APPENDIX A: DERIVATION OF THE SHAPE EQUATIONS FOR CLOSED DNA

The axis of the molecule (the ribbon) is parametrized using spherical coordinates for the tangent vector

$$\mathbf{t} = (\sin\theta\cos\phi, \sin\theta\sin\phi, \cos\theta) \quad . \tag{A1}$$

In this parametrization, the functional F' defined in Eq. (10) can be written as

$$F' = B\int_0^{S_0} L\, dS \quad , \tag{A2}$$

with the Lagrange function

$$L(\theta,\dot\theta,\ddot\theta,\phi,\dot\phi,\ddot\phi) \equiv \left[\frac{1}{2}(\dot\phi^2\sin^2\theta+\dot\theta^2) + \bar\gamma\left(\sin\theta\frac{\dot\phi^3\cos\theta\sin\theta+\dot\phi\ddot\theta-\dot\theta\ddot\phi}{\dot\phi^2\sin^2\theta+\dot\theta^2} - 2\dot\phi\cos\theta\right)\right.$$
$$\left. +\bar N_x(\dot x-\sin\theta\cos\phi) + \bar N_y(\dot y-\sin\theta\sin\phi) + \bar N_z(\dot z-\cos\theta)\right] \quad . \tag{A3}$$

Here $\bar\gamma \equiv \gamma/(2\pi B)$ and $\bar{\mathbf{N}} \equiv \mathbf{N}/B$. In the following, we choose a coordinate system with $N_x = N_y = 0$ and $\mathbf{N} = (0,0,N_z)$. This condition can always be achieved by a rotation.

The Euler-Lagrange equations

$$\frac{\partial L}{\partial\phi} - \frac{d}{dS}\frac{\partial L}{\partial\dot\phi} + \frac{d^2}{dS^2}\frac{\partial L}{\partial\ddot\phi} = 0,$$
$$\frac{\partial L}{\partial\theta} - \frac{d}{dS}\frac{\partial L}{\partial\dot\theta} + \frac{d^2}{dS^2}\frac{\partial L}{\partial\ddot\theta} = 0 \tag{A4}$$

follow from the condition $\delta F' = 0$. Inserting the expression (A3) for L into (A4), one obtains the shape equations for closed DNA, which read

$$\ddot\phi\sin\theta + 2\dot\phi\dot\theta\cos\theta + \bar\gamma\dot\theta = 0,$$
$$\ddot\theta - \dot\phi^2\cos\theta\sin\theta + \bar N_z\sin\theta - \bar\gamma\dot\phi\sin\theta = 0 \quad . \tag{A5}$$

Note that all terms containing derivatives of third and fourth order cancel. Similar shape equations have been derived in Ref. [7] by a less straightforward method. The bending energy E_B for given writhing number $\mathcal{W}$ as shown in Fig. 2 has been obtained by solving Eqs. (A5) and inserting the resulting shapes into (5) and (9).

APPENDIX B: SELF-INTERACTION OF THE ROD

Shapes of lowest bending energy with $\mathcal{W} > 1$ in general do self-interact. For small rod diameter $a \simeq 0$,

self-contact of self-interacting configurations occurs at a point along the shape. We assume that this point of self-contact is the center of symmetry of the shape. Therefore, it is sufficient to study a segment of length $S_0/2$ with both ends fixed at the point of self-contact. This segment is shown by a solid line in Fig. 3(b).

The boundary conditions at both ends of this segment have to guarantee the symmetry and the stationarity of the complete shape taking the constraint of self-avoidance into account. The variation of the functional F' for variations at one boundary reads

$$\frac{\delta F'}{B} = \left(\frac{\partial L}{\partial \dot{\phi}} - \frac{d}{dS}\frac{\partial L}{\partial \ddot{\phi}}\right)\delta\phi + \frac{\partial L}{\partial \ddot{\phi}}\delta\dot{\phi} + \left(\frac{\partial L}{\partial \dot{\theta}} - \frac{d}{dS}\frac{\partial L}{\partial \ddot{\theta}}\right)\delta\theta + \frac{\partial L}{\partial \ddot{\theta}}\delta\dot{\theta} + \frac{\partial L}{\partial \dot{\mathbf{R}}}\delta\mathbf{R} \quad . \tag{B1}$$

Inserting the expression (A3) into (B1) leads to

$$\frac{\delta F'}{B} = (\dot{\phi}\sin^2\theta - \bar{\gamma}\cos\theta)\delta\phi - \frac{\bar{\gamma}\dot{\theta}\sin\theta}{\dot{\phi}^2\sin^2\theta + \dot{\theta}^2}\delta\dot{\phi} + \left(\dot{\theta} - \frac{\bar{\gamma}\dot{\phi}\dot{\theta}\cos\theta}{\dot{\phi}^2\sin^2\theta + \dot{\theta}^2}\right)\delta\theta + \frac{\bar{\gamma}\dot{\phi}\sin\theta}{\dot{\phi}^2\sin^2\theta + \dot{\theta}^2}\delta\dot{\theta} + \bar{N}_Z\delta Z \quad , \tag{B2}$$

where $\delta\phi$, $\delta\theta$, $\delta\dot{\phi}$, $\delta\dot{\theta}$, and δZ denote the variations of the angles ϕ and θ, their derivatives $\dot{\phi}$ and $\dot{\theta}$, and the Z coordinate at the corresponding boundary. The boundary conditions for self-interacting shapes can now be derived from Eq. (B2). For the segment of length $S_0/2$, they read

$$\mathbf{R}(0) = \mathbf{R}(S_0/2) = \mathbf{0}, \tag{B3}$$

$$\theta(0) = \theta(S_0/2) = \pi/2, \tag{B4}$$

$$\phi(0) = \pi - \phi(S_0/2), \tag{B5}$$

$$\dot{\theta}(0) = \dot{\theta}(S_0/2), \tag{B6}$$

$$\dot{\phi}(0) = \dot{\phi}(S_0/2) = 0 \quad . \tag{B7}$$

Equation (B3) fixes both ends in the point of self-contact and Eq. (B5) fixes the orientation of the shape in the X-Y plane. Stationarity with respect to δX and δY follows from $N_X = 0$ and $N_Y = 0$. Variations δZ are suppressed by self-avoidance; see Fig. 3(b). Equations (B4)–(B7) are required by the symmetry of the shape. In terms of boundary variations, Eqs. (B4) and (B7) correspond to $\delta\theta = 0$ and $\delta\dot{\phi} = 0$. If all these relations are inserted into Eq. (B2), the boundary variation $\delta F'$ vanishes. Therefore the corresponding solutions are stationary with respect to variations of the shape. Using these boundary conditions, the branch of nonplanar self-interacting shapes, with $1 < \mathcal{W} < 2$ as discussed in Sec. IV B, has been obtained.

[1] L. Stryer, *Biochemistry* (Freeman, New York, 1988).

[2] J. White, in *Mathematical Models in DNA Sequencing*, edited by S. Wassermann (CRC, Baton Rouge, 1989).

[3] F.B. Fuller, Proc. Natl. Acad. Sci. U.S.A. **75**, 3557 (1978).

[4] W. Keller, Proc. Natl. Acad. Sci. U.S.A. **72**, 2250 (1975).

[5] C. Benham, in *Mathematical Models in DNA Sequencing* (Ref. [2]).

[6] C. Benham, Phys. Rev. E **39**, 2582 (1989).

[7] C. Benham, Biopolymers **18**, 609 (1979); **22**, 2477 (1983).

[8] E. Guitter and S. Leibler, Europhys. Lett. **17**, 643 (1992).

[9] M. LeBret, Biopolymers **18**, 1709 (1979).

[10] T. Schlick and W.K. Olson, J. Mol. Biol. **223**, 1089 (1992); Y. Yang, I. Tobias, and W.K. Olson, J. Chem. Phys. **98**, 1673 (1993).

[11] M.D. Barkley and B.H. Zimm, J. Chem. Phys. **70**, 2991 (1979).

[12] M.T. Record *et al.*, Annu. Rev. Biochem. **50**, 997 (1981).

[13] J. White, Am. J. Math. **91**, 693 (1969).

[14] L.D. Landau and E.M. Lifshitz, *Theory of Elasticity*, 2nd ed. (Pergamon, Oxford, 1970).

[15] W.R. Bauer, Ann. Rev. Biophys. Bioeng. **7**, 287 (1978).

[16] W.F. Pohl, J. Math. Mech. **17**, 975 (1968).

[17] Under continuous deformations of a closed space curve, the value of the self-linking number can change discontinuously by an integer amount.

[18] For molecular thickness $a = 0$, the axes of the self-interacting shapes self-intersect. The writhe of these shapes is defined to be the limiting value of $\mathcal{W}$ for $a \to 0$.

[19] Note that $E_B(\mathcal{W}) = E_B(-\mathcal{W})$, which follows from the symmetry of the energy F with respect to inversions $\mathbf{R} \to -\mathbf{R}$. Under an inversion, the writhe transforms as $\mathcal{W} \to -\mathcal{W}$.

[20] This method has been introduced in the context of curvature models for vesicle shapes, where a generalized Legendre transformation is used to map the energies of stationary shapes within different curvature models; see L. Miao, U. Seifert, M. Wortis, and H.G. Döbereiner, Phys. Rev. E (to be published).

[21] The phase diagram does not depend on the sign of $\Delta\mathcal{L}$ since the energy E obeys $E(\Delta\mathcal{L}) = E(-\Delta\mathcal{L})$. This follows from the symmetry of E_B [19] and Eq. (13).

[22] P.J. Hagermann, Annu. Rev. Biophys. Chem. **17**, 265 (1988).

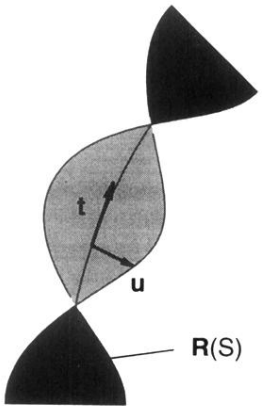

FIG. 1. Twisted ribbon as a model for the geometrical properties of DNA. The central line of the ribbon follows the molecular axis with coordinates $\mathbf{R}(S)$ parametrized by the arclength S. Two unit vectors are defined along the axis: the tangent vector $\mathbf{t}$ and the vector $\mathbf{u}$ perpendicular to $\mathbf{t}$ which points to the edge of the ribbon.